Biomicrofluidics

Cell counting and velocity algorithms for hydrodynamic study of unsteady biological flows in micro-channels

Cite as: Biomicrofluidics **17**, 014105 (2023); https://doi.org/10.1063/5.0138587
Submitted: 13 December 2022 • Accepted: 20 December 2022 • Published Online: 23 January 2023

Federica Torrisi, Giovanna Stella, Francesca M. Guarino, et al.

Biomicrofluidics ARTICLE scitation.org/journal/bmf

Cell counting and velocity algorithms for hydrodynamic study of unsteady biological flows in micro-channels

Cite as: Biomicrofluidics **17**, 014105 (2023); doi: 10.1063/5.0138587
Submitted: 13 December 2022 · Accepted: 20 December 2022 ·
Published Online: 23 January 2023

Federica Torrisi,[1] Giovanna Stella,[1,a)] Francesca M. Guarino,[2] and Maide Bucolo[1]

AFFILIATIONS

[1]Department of Electrical, Electronic and Computer Engineering, University of Catania, 95125 Catania, Italy
[2]Department of Biomedical and Biotechnological Sciences, University of Catania, 95125 Catania, Italy

[a)]**Author to whom correspondence should be addressed:** giovanna.stella@phd.unict.it

ABSTRACT

In this paper, the combination of two algorithms, a cell counting algorithm and a velocity algorithm based on a Digital Particle Image Velocimetry (DPIV) method, is presented to study the collective behavior of micro-particles in response to hydrodynamic stimuli. A wide experimental campaign was conducted using micro-particles of different natures and diameters (from 5 to 16 μm), such as living cells and silica beads. The biological fluids were injected at the inlet of a micro-channel with an external oscillating flow, and the process was monitored in an investigated area, simultaneously, through a CCD camera and a photo-detector. The proposed data analysis procedure is based on the DPIV-based algorithm to extrapolate the micro-particles velocities and a custom counting algorithm to obtain the instantaneous micro-particles number. The counting algorithm was easily integrated with the DPIV-based algorithm, to automatically run the analysis to different videos and to post-process the results in time and frequency domain. The performed experiments highlight the difference in the micro-particles hydrodynamic responses to external stimuli and the possibility to associate them with the micro-particles physical properties. Furthermore, in order to overcome the hardware and software requirements for the development of a real-time approach, it was also investigated the possibility to detect the flows by photo-detector signals as an alternative to camera acquisition. The photo-detector signals were compared with the velocity trends as a proof of concept for further simplification and speed-up of the data acquisition and analysis. The algorithm flexibility underlines the potential of the proposed methodology to be suitable for real-time detection in embedded systems.

I. INTRODUCTION

Up to date, the most sophisticated laboratory equipment ensuring a complete analysis of particles in suspension is a Flow Cytometer.[1] It is routinely used in diagnostic and research fields to detect physical and chemical features of cells[2] and to count them.

In this paper, the combination of two algorithms, a cell counting algorithm and a velocity algorithm based on a Digital Particle Image Velocimetry (DPIV) method, is presented to investigate the collective behavior of particles, in micro-channels or chambers, in response to hydrodynamic stimuli. The proposed data analysis procedure offers the advantage to extract automatically the information on the number of particles, flowing in an investigated area in time, and their velocities. A set of experiments were carried out to validate the method proposed in this paper and the results obtained show a significant variation in the hydrodynamic responses to external stimuli and the possibility to associate them with the particles' physical properties. The simplified optical setup and the algorithm flexibility, make this methodology suitable for real-time detection in embedded systems for the study of cell interaction, as in the Lab-on-a-Chip. A microfluidic-based system able to detect variations in number, concentration, and shape of particles as well as their hydrodynamic properties would considerably improve the identification of various physiological and pathological conditions. The consistency of a biological fluid may change depending on the intrinsic properties of the particles and fluids used, or alterations induced by a disease of the organisms examined may occur. The blood is an example, which is composed of cells with distinguishable traits like size, shape, surface characteristics, compactness, and plasma composition.[3] All these listed items affect the differentiated migration dynamics of specific blood particles/cells. Some

pathological diseases, such as atherosclerosis or thrombosis, can be associated directly with blood disorders altering the cells' movement, whereas others, like anemia or leukemia, affect the cells' proliferation and indirectly the flow.[4,5]

For over a century, manual cell counting with the use of a cytometer and a microscope has been the prevalent technique in laboratories, despite requiring bulky equipment and being a time-consuming approach. As an alternative to manual counting, automated cell counters based on the Coulter Counter principle have been developed and become commercially available.[6] The limits in their use are to require bulky and costly equipment and a large number of samples and reagents. Advances in microfluidics have shown promising results in the development of low-cost and portable Lab-on-a-Chip devices with higher throughput, sensitivity, and accuracy.[7–9] In the miniaturization efforts, different technological issues have arisen in relation to the biological or chemical application contexts[10–13] and to the detection approaches.[14–17] It is significant to mention the recent advancement in the use of microfluidics for the study of physiological processes as in the case of organs-on-chip,[18,19] and in biology as for the cellular analysis[20,21] and cell-to-cell interactions.[22]

This work aims to develop an approach for the investigation of micro-particles moving in micro-channels or chambers suitable for Lab-on-a-Chip implementation. To do that, a wide experimental campaign was carried out, using micro-particles of different natures, as living cells and silica beads, and with different physical properties, such as density and size (from 5 to 16 μm). An external oscillating flow was imposed at the inlet of a micro-channel and the process was continuously monitored in a test area simultaneously by using a CCD camera and a photo-detector. The videos and the signals acquired were analyzed to determine information correlated to the changes in time of the micro-particles number and their velocities.

The application of flow visualization in biological systems is becoming increasingly common in studies ranging from intracellular transport to the movements of whole organisms. In cell biology, the standard method for measuring cell-scale flows and/or displacements has been Digital micro Particle Image Velocimetry (micro DPIV).[23–25] More and more researchers are recently looking to live-cell imaging to provide a quantitative understanding of cellular mechanisms. In Ref. 26, a quantitative phase velocimetry (QPV) approach, which uses the principle of PIV, was developed to track the velocity flow of material within a single cell, and in Ref. 27, a live scanning particle-imaging velocimetry (LS-PIV) was implemented to quantify the blood velocity in live mice suffering from a cerebral arteriovenous malformation. They detect the blood velocities and exaggerated pulsatility along the abnormal vascular network in these animals. In Ref. 28, a free and open-source solution for performing efficient and robust quantification of collective cellular migration in the increasingly popular 3D dynamic data sets in life sciences are developed. In Ref. 29, the PIV approach was used for analyzing the dynamics of *in vivo* models of collective migration. That evidences the relevance of the topics and the challenging open issues around them and the effort in finding a straightforward methodology for velocity cell detection.

In this work, the micro-particle velocities were computed by taking into account the DPIV method based on image analysis, and the micro-particles number was obtained by a custom counting algorithm. The DPIV methodology was initially used by the authors to study the collective behaviors of RBCs in a micro-channel in unsteady conditions.[30,31] Starting from that, in this paper, a further development of this approach is presented to extract automatically the information on the number of particles, flowing in an investigated area in time, and to detect their velocities. Working in the MATLAB environment, it was possible to easily integrate the counting algorithm with the DPIV-based algorithm, to automatically run the analysis to different videos, and to post-process the results in time and frequency domain, showing the suitability for automatic classification of micro-particles in biological fluids. In the considered experiments, it was possible not only to detect the hydrodynamic behavior of the micro-particles, but also to correlate this to their physical features, such as the size and the density of micro-particles.

In the last few decades, image processing-based methods[32–35] and microfluidics-based systems for particle counting and detection have been developed to overcome the barriers associated with conventional methods,[36,37] but the use of real-time image processing is still very challenging[38] due to hardware and software requirements. In order to overcome these issues for the development of a real-time approach, in this work, the possibility to detect the flows by the use of photo-detector signals as an alternative to camera acquisition has also been investigated. The optical detection by signals was proved to be useful for characterizing the flow non-linearity,[39,40] it was possible for the development of a real-time velocity detection system for the slug flow analysis in a micro-channel[41] and the realization of a micro-optofluidic flow detector for the investigation of biological and chemical samples on chip.[42]

In this paper, the signals, collected by the photo-detector, were compared with the velocity trends obtained by the DPIV-based algorithm as a proof of concept for a further simplification and speed-up of the data acquisition and analysis, based on a simpler optical detection than the video recording needed for the on-chip implementation. The paper is organized as follows: Sec. II describes in detail the experimental setup, the campaign carried out and illustrates the procedures implemented to count the micro-particles and calculate their velocity. Section III presents the results obtained from the counting of the micro-particles, the trends obtained from the DPIV-based algorithm and their correlation, the comparison between the velocity trends obtained from the DPIV-based algorithm and the signals obtained from the photo-detectors, and finally the hydrodynamic responses of the micro-particles in the time and frequency domains under different experimental conditions, discussing their correlation with the properties of the micro-particles.

II. MATERIALS AND METHODS

A. Experimental setup

The experimental setup is composed of a syringe pump, a microfluidic chip, and an opto-mechanical system. The syringe pump (neMESYS low-pressure module, Cetoni GmbH, Korbussen, Germany) was used to inject a fluid mixed with micro-particles in a Y-junction squared rectilinear micro-channel in cyclo-olefin copolymer (SMS0104, Thinxxs, Zweibrücken, Germany), with a

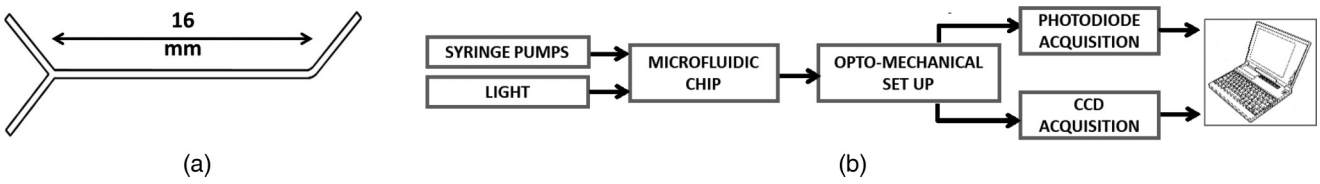

FIG. 1. (a) The Y-junction squared rectilinear micro-channel with a diameter of 320 μm and (b) the flow chart of the experimental setup.

length of 16 mm and a square cross section with a side of 320 μm. Its geometry is shown in Fig. 1(a). The microfluidic process was analyzed in an investigated area at a distance of 8 mm from the inlet, illuminated by a white light. A photo-detector, labeled PH (SM05PD1A, Thorlabs, Newton, NJ, USA), with an operating wavelength of 350–1100 nm, connected to an acquisition board (BNC-2110, National Instruments, Austin, TX, USA) and a CCD camera (DCU224, Thorlabs, Newton, NJ, USA), with a resolution of 1280 × 1024 pixels (pixel size of 4.65 μm, square), included both in the opto-mechanical system (Thorlabs, Newton, NJ, USA) allow a simultaneous process monitoring. A magnification of 10x (PLN, Olympus, Tokyo, Japan), with a numerical aperture (NA) of 0.25, a working distance of 10.6 mm, and a depth of focus of 440 μm has been used. A distance of 3.5 mm between the focal plane and the objective has been considered and due to the geometry of the micro-channel being square-sectioned, there is no loss of visual field, as is usual the case with cylindrical micro-channels.[43] A PC with Intel® Core™ i7-6500U CPU @ 2.50 GHz 2.59 GHz, RAM 8 Gb and operative system 64 bit was used for the analysis.

The data were recorded for about 75 s, with a video frame rate of 60 frames per second, around 4.500 frames per experiment, and a sampling frequency of 1 kHz for the photo-detector acquisition. A detailed description of the opto-mechanical setup is reported in Ref. 44. A flow chart and some pictures of the experimental setup are shown in Figs. 1(b) and 2(a). In particular, Figs. 2(b) and 2(c) show a zoom of the micro-channel together with the objective lens and a zoom of the photo-detector position with an image of the photo-detector used. In Fig. 3, a scheme showing the CCD resolution, the photo-detector resolution, and the region of interest (ROI) selected in the performed experiments and analyzed is shown.

B. Experimental campaigns

The microfluidic chip was fed by an oscillating flow. The biological fluids employed for the experiments were obtained by diluting some micro-particles in a saline solution, the phosphate buffered saline (PBS, a density of 1072 kg/m^3). The micro-particles diluted with the PBS were of two types: live cells and artificial beads. The live cells, of eukaryotic origins, were the yeast cells of *Saccharomyces cerevisiae* and the human epithelial *HeLa* cells. The relevant difference between these two types of cells concerns their dimension: the yeast cells have a diameter of 5 μm while the human cells have a diameter of 16 μm. The artificial beads were silica beads with a diameter of 6 μm. The number concentration of particles, diluted in 10 ml of PBS fluid, was 1×10^5 for the silica beads, 1×10^7 for human cells, and 1×10^8 for the yeast cells. The physical properties of the particles, such as mass, radius, volume, and density, are summarized in Table I.

Initially, a single-phase PBS flow, in the absence of micro-particles, was recorded to quantify the effect of the fluid background in the images and the signals. The PBS flow was injected at the inlet with an oscillating flow at a frequency of $f_i = 0.1$ Hz and an amplitude of $A = 0.1$ ml/min. The following 22 experiments conducted are summarized per type of cells in Table II. The micro-particles flow was fed into the micro-channel using an oscillating flow at a frequency of $f_i \in \{0.1; 0.2\}$ Hz and an amplitude strength varying in the range $A \in \{0; 0.2\}$ ml/min. For the three categories of particles, five equal experimental conditions were considered with $f_i = 0.1$Hz and $A \in \{0.04; 0.05; 0.07; 0.1; 0.15\}$ ml/min. Then, for the yeast cells, the campaign was extended considering three other experiments with $f_i = 0.1$ Hz and $A \in \{0; 0.03; 0.2\}$ ml/min and four experiments with $f_i = 0.2$ Hz and $A \in \{0.05; 0.07; 0.1; 0.2\}$ ml/min.

C. Micro-particle counting algorithm

In diagnostic and research life science laboratories, cell counting is a common task for any cell-based assay. The less expensive procedure is to count the cells using a reusable hemocytometer by visualizing them with a bright field optical microscope.[45] To reduce the systematic and random error of the manually count and to improve the statistic values, these approaches have been automated with micro-particles imaging analysis acquisition based on enhanced technologies and paired with a sophisticated micro-particles counting algorithm.

The proposed procedure provides a continuous counting in time of the micro-particles number in the investigated area, avoiding any manual and individual selecting of the frames to be studied. It analyzes automatically the video, frame by frame, counts the number of particles per frame, and collects this information in a signal.

The micro-particles counting algorithm was implemented in the MATLAB environment and the fundamental steps implemented are listed in the flow chart in Fig. 4. The images, to be analyzed, are loaded automatically in the platform and the first step is the definition of the ROI in the images, which will be taken into account for all the duration of the analysis.

After the ROI definition, each image (defined as variable "image") is converted into the grayscale (defined as "*gray_image*") by using the function "rgb2gray(image)." In addition, to adjust the images' intensity values to the grayscale images, the function "imadjust(*gray_image*)" is applied. Then, a Gaussian filter is

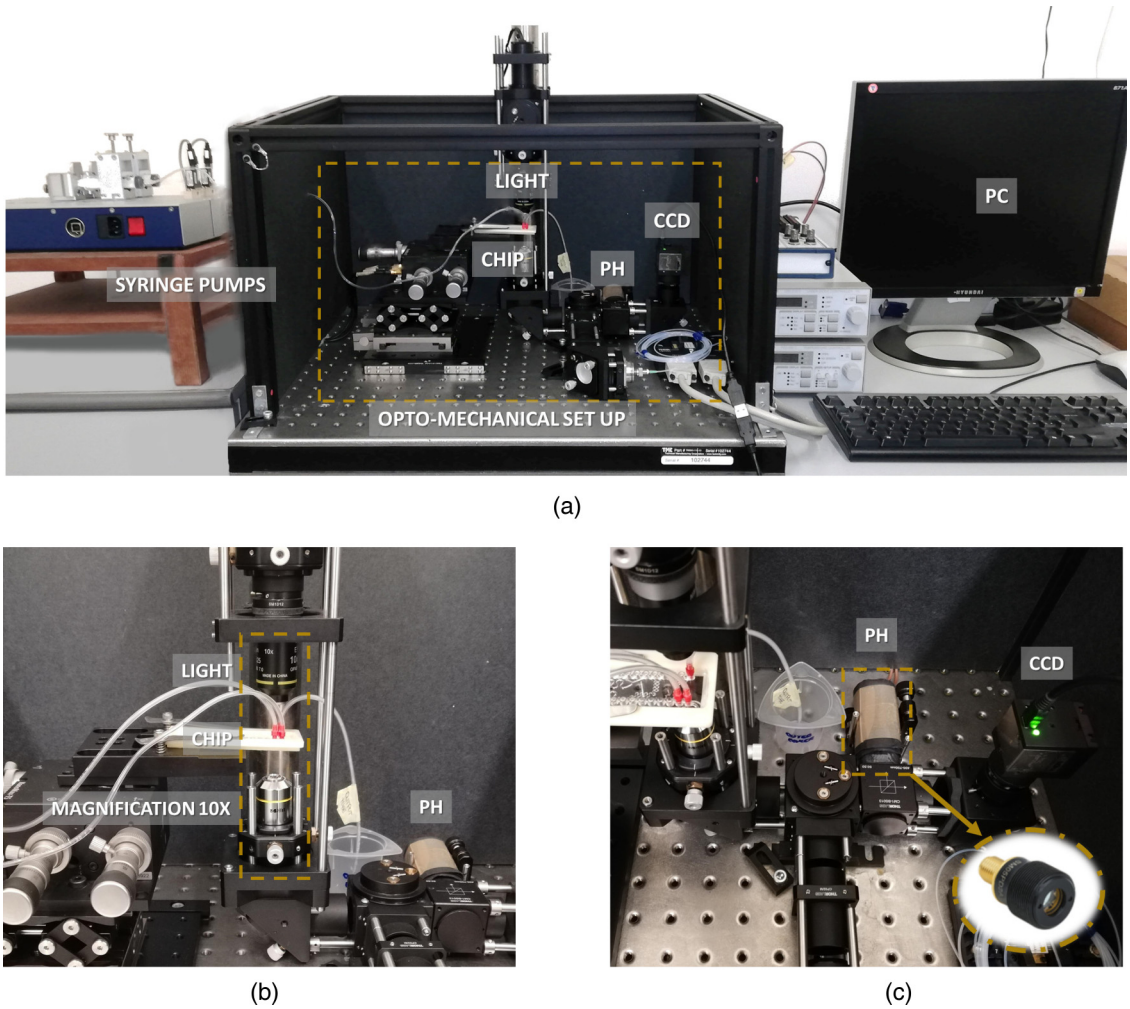

FIG. 2. (a) Picture of the opto-mechanical experimental setup. (b) Closer picture showing the chip in which it is included the rectilinear micro-channel together with the 10x magnification system and the illumination system. (c) Closer picture of the photo-detector position and a cartoon of the photo-detector used for monitoring the micro-particles flow.

applied to the new images, by using the function "imgaussfilt (*gray_image*, σ)," to smooth the images and reduce the noise ("*filtered_image*"). The arguments of this last function are the grayscale images ("*gray_image*") to be filtered and sigma ($\sigma = 5$), which is the standard deviation of the Gaussian distribution and defines the filter size. The difference between the grayscale and the filtered images contains the noise removed in the filtering phase ("*diff_image*"). However, the locations of the micro-particles are still visible in these noise images as regions of increased variability. At this point, the new images ("*diff_image*") must be converted into binary images ("*binary_image*"), by using the function "imbinarize(*diff_image*, th1)," which creates binary images by selecting a threshold value automatically and variable at each circumstance ("th1 = graythresh(*diff_image*")). All the values above the threshold will be replaced with 1 and all the others with 0. As mentioned before, the threshold ("th1") is not a fixed value, but changes for every image, and it is calculated through the function "graythresh(*diff_image*)." Finally, the function "bwboundaries (*binary_image*,"noholes")" was used to trace the exterior boundaries of objects in the binary images. The arguments of this function are binary images ("*binary_image*") and the "noholes" option, which specifies searching only the boundaries of objects by excluding noholes, providing better performance. The function returns a cell array ("[B,L,N]") with the boundaries pixel locations ("B"), a label matrix ("L") where the objects are labeled and the number of micro-particles found ("N"). After that, a check on the detected micro-particles is carried out, to eliminate possible artifacts. With the function "regionprops (L,"Area,""Centroid")," it is possible to

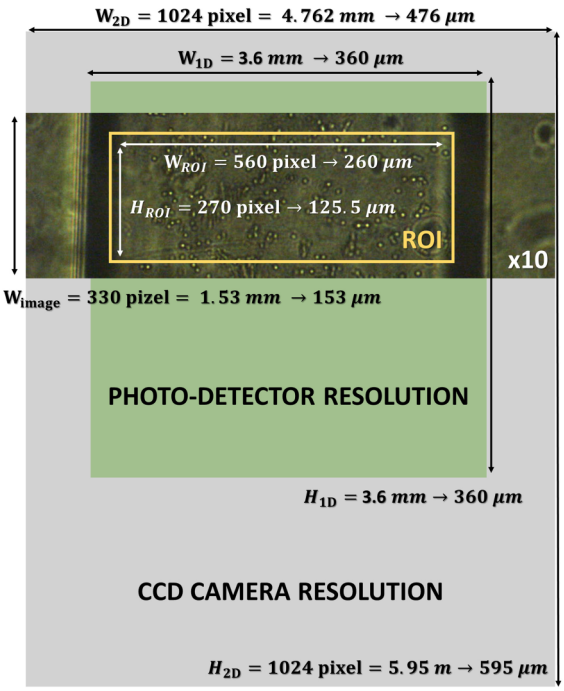

FIG. 3. Picture showing the CCD resolution, the photo-detector resolution, and the region of interest (ROI) acquired and analyzed in the performed experiments.

measure some micro-particle properties such as the area, the center, and the circularity. Therefore, it is possible to verify if the detected particles have an appropriate area, consistent with the micro-particle size investigated, defining the minimum and maximum dimensions of the searched objects in pixels, to count among the found micro-particles only those that have an appropriate size. For the silica beads and the yeast cells, the minimum area was set to 1 pixel and the maximum area to 2 pixels. For the human cells, the minimum area to 3 pixels and the maximum area to 4 pixels. There is another threshold parameter ("th2") that needs to be set based on the shape of the objects. In the experimental campaigns carried out, due to the circular geometry of the micro-particles investigated, the threshold parameter ("th2") was set to 1, to indicate a perfect circle. It is possible to set this threshold differently based on the requirement of the analysis. After defining this parameter, the exterior boundaries of particles are traced and the number of particles is found.

TABLE II. The experimental campaigns.

Micro-particles	Frequency f_i (Hz)	Amplitude A (ml/min)
Yeast cells	0.1	0, 0.03, 0.04, 0.05, 0.07, 0.1, 0.15, 0.2
	0.2	0.05, 0.07, 0.1, 0.2
Human cells	0.1	0.04, 0.05, 0.07, 0.1, 0.15
Silica beads	0.1	0.04, 0.05, 0.07, 0.1, 0.15

Using the presented algorithm, the same for all the micro-particles investigated, the detection of micro-particles results to be simple, fast, and accurate.

D. Micro-particle DPIV-based algorithm

The data acquired in video format were processed by a DPIV-based automatic algorithm to have instantaneous velocity measurements and visualizations. The time-varying velocity vector maps obtained, showing the displacements of the particles in time in an investigated area, were then processed to extract the mean of the migration velocity per experiment. Thanks to this approach, the complexity of the standard Flow Cytometer equipment is shifted in the algorithm implementation.

Initially, each video is decomposed into frames and a specific ROI is set. The ROI is the portion of the monitored area that was considered for the hydrodynamic cell flow investigation. The ROI was set equal for the experiments using the same cells. The DPIV analysis was conducted by a three-passes discrete Fourier transform (DFT) in frequency domain as implemented by the PIVlab tool.[46] The three interrogation areas in pixel were chosen as follows: $Area1 = 64$, $Area2 = 32$, and $Area3 = 16$. The step size of the sampling window used in the DPIV method to calculate the velocities of the micro-particles was set to half of the last interrogation area (Area3 = 16 pixels), resulting in a step size of 8 pixels. The details of the DPIV setting have already been presented by the authors in Ref. 30.

In Fig. 5, the algorithm steps from the extraction of the video frames to the computation of the micro-particle velocity trends are presented. On the left three frames, one per cell type are reported, respectively, for the yeast cells (5 μm), the human cells (16 μm), and the silica beads (6 μm). The ROI selected is highlighted in yellow. On the right, for the human cells, a frame at a time instant $\bar{t}$ of the time-varying velocity vector map $V(i, j, \bar{t})$ with i and j referring to the i^{th}apex and j^{th}apex pixel position in the image ROI, obtained by the DPIV processing, is considered. The velocity

TABLE I. The physical properties of the micro-particles.

Micro-particles	Mass (kg)	Radius (m)	Volume (m^3)	Density ($\frac{kg}{m^3}$)
Yeast cells	7.37×10^{-14}	2.5×10^{-6}	6.54×10^{-17}	1126
Human cells	2.23×10^{-12}	8.0×10^{-6}	2.14×10^{-15}	1040
Silica beads	1.36×10^{-13}	3.0×10^{-6}	1.13×10^{-16}	1200

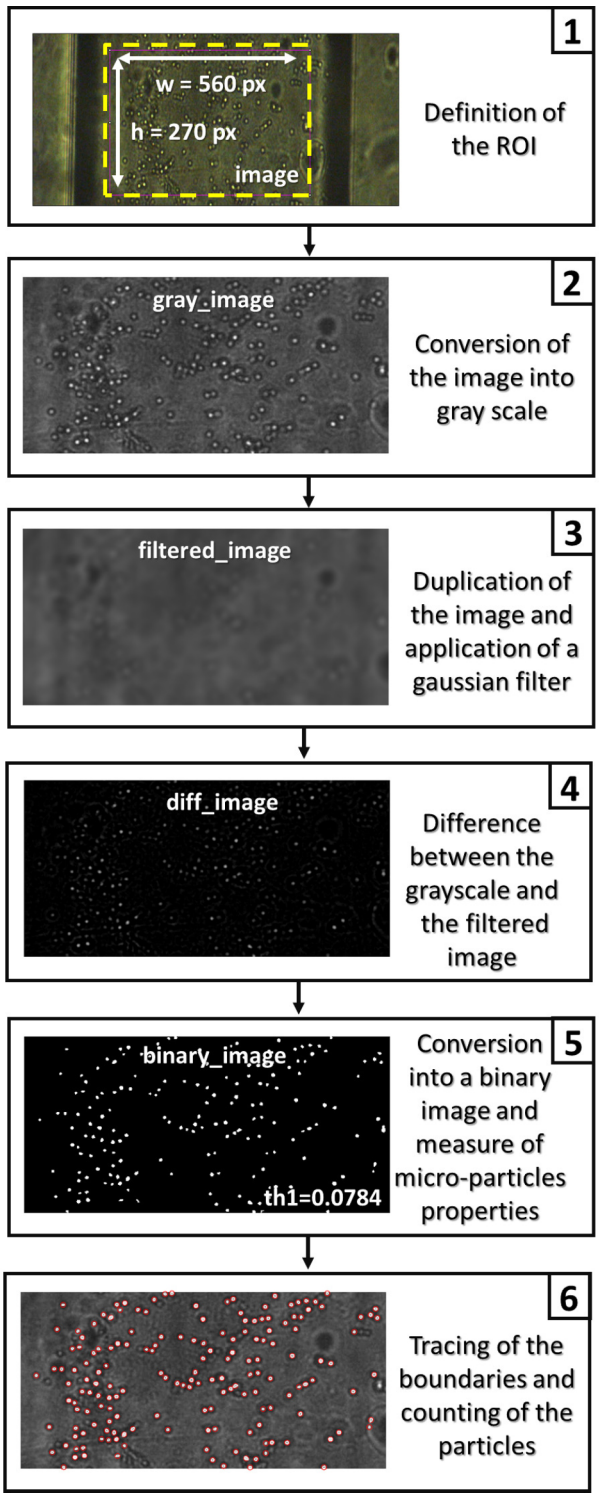

FIG. 4. The flow chart of the algorithm implemented to count the micro-particles in the MATLAB environment.

spatial distribution on the horizontal and vertical directions are $V_x(i, j, \bar{t})$ and $V_y(i, j, \bar{t})$, respectively. Finally, those are spatially averaged, in order to obtain the mean velocity values $\langle V_x(\bar{t})\rangle$ and $\langle V_y(\bar{t})\rangle$. This procedure repeated for all the frames of the time-varying vector map gives two signals representing the mean velocity trends on x and y directions vs time, respectively $\langle V_x(t)\rangle$ and $\langle V_y(t)\rangle$ obtained as shown in Eqs. (1) and (2),

$$\langle V_x(t)\rangle = \frac{1}{m}\sum_{i=1}^{nx}\sum_{j=1}^{ny} V_x(i, j, t), \tag{1}$$

$$\langle V_y(t)\rangle = \frac{1}{m}\sum_{i=1}^{nx}\sum_{j=1}^{ny} V_y(i, j, t), \tag{2}$$

where nx and ny are the number of pixels along the horizontal and vertical region of interest dimensions and $m = nx \cdot ny$ is the total number of pixels in the region of interest analyzed. Looking at the movement of the micro-particles along the micro-channel and based on the image orientation, the dominant velocity component is the vertical one. The micro-particle flows flowed from the top to the bottom of the investigated area and vice versa. In particular, the trend of the vertical velocity component $\langle V_y(t)\rangle$ shows the periodicity of the oscillating input flow imposed and no-periodicity can be detected in the trend of the horizontal velocity component $\langle V_x(t)\rangle$. For this reason, the following analysis is related to the $\langle V_y(t)\rangle$.

The different number of particles in the investigated area can significantly influence the velocity value obtained by the DPIV algorithm; therefore, the velocity signals were normalized to the average number of particles obtained by the implemented micro-particle counting algorithm, described in detail in Sec II C. In particular, this normalization was applied due to the fact that the density of micro-particles in each experimental condition was different, by applying a normalization it is possible to compare the results obtained. The micro-particles hydrodynamic response in time domain was evaluated by computing the range of the velocity signal $\langle V_y(t)\rangle$, as in Eq. (3),

$$Range\langle V_y(t)\rangle = \max(\langle V_y(t)\rangle) - \min(\langle V_y(t)\rangle). \tag{3}$$

Then, the values of the velocity range ($Range\langle V_y(t)\rangle$) per experiment were normalized with respect to the average number of micro-particles ($\langle N_p(t)\rangle$) computed in the investigated area per experiment.

III. RESULTS AND DISCUSSION

A. Trend of micro-particle counting and velocity

The two algorithms were used to analyze the data collected in the experimental campaigns, allowing to investigate how the hydrodynamic response of the micro-particles could be correlated with their physical properties and characterize their collective behavior. To compare the results obtained for different cell types, the average number of micro-particles $\langle N_p(t)\rangle$ and the velocity signals $\langle V_y(t)\rangle$ per experiment, computed by the counting algorithm described in

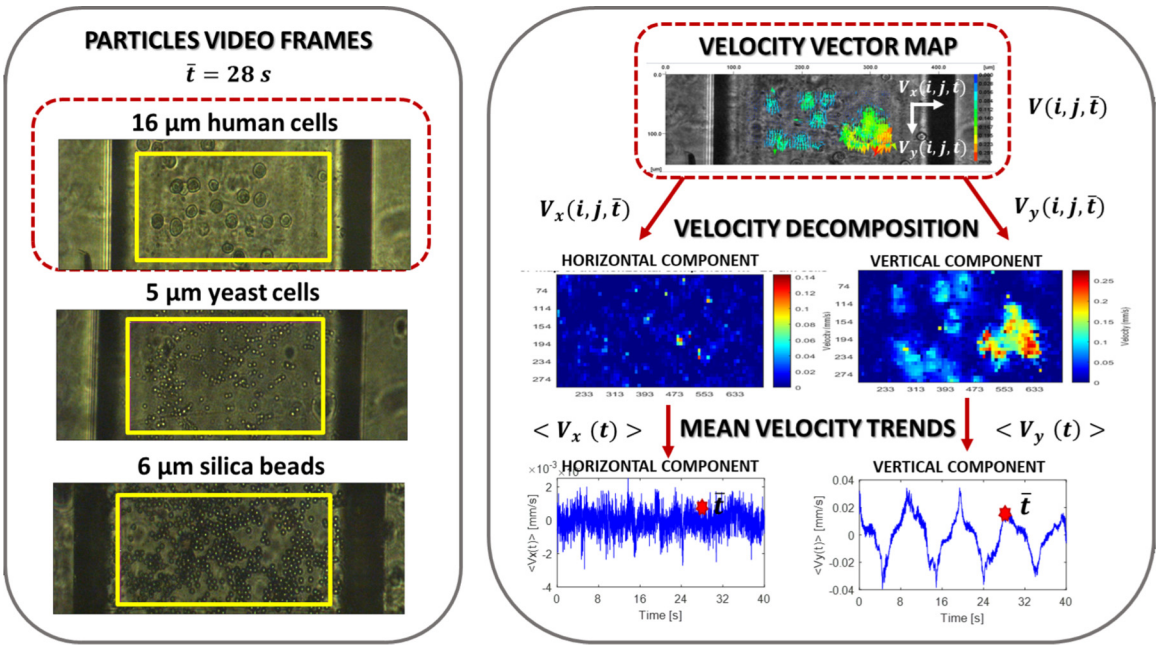

FIG. 5. The algorithm steps of the procedure for the video processing based on DPIV analysis. On the left column, the extraction of the video frames. On the right column for the human cells, in sequence the instantaneous velocity vector maps $V(i, j, \bar{t})$, its decomposition in the horizontal and vertical velocity components $\{V_x(i, j, \bar{t}), V_y(i, j, \bar{t})\}$, and the mean velocity trends $\{\langle V_x(t)\rangle, \langle V_y(t)\rangle\}$.

Sec. II C and the DPIV-based algorithm described in Sec. II D, were considered. The computational time required for the analysis of 1000 video frames was 2 min for the counting algorithm and 1 h for the DPIV-based algorithm.

In Fig. 6, for human cells and yeast cells in the experimental condition with $\{A = 0.1\,\text{ml/min}, f_i = 0.1\,\text{Hz}\}$ in a time interval of about 16 s, the frames with the micro-particles detected and the signals $N_p(t)$ reconstructed by counting instantaneously the number of micro-particles over time are plotted.

It was noted that the counting of micro-particles becomes more difficult with the standard platform, when the color within the particle is similar to the background and the micro-particle boundaries cannot be properly defined, as in the case of human cells ($16\,\mu$m). This has been overcome by the proposed algorithm, as the analyzed frame in Fig. 6(a) shows.

For its validation, the results obtained were compared with the one of a standard platform *ImageJ*,[47] widely used in this field for particle counting single images. The steps performed in both the cases are similar. Twelve frames per experiment (four in the first part of video, four in the last part, and four in the middle) were selected and the number of micro-particles counted with the following methods: the *ad hoc* counting algorithm presented in this paper, the standard method through ImageJ, and manually. Considering the experiments with yeast cells and silica beads, the variation detected between the two methods was of the order of 10% in favor of the proposed *ad hoc* micro-particle counting. Compared to manually counted micro-particles, there is a 2% difference with the proposed *ad hoc* micro-particle counting algorithm.

The mean number of all the micro-particles, counted by the implemented algorithm for each experiment, is reported in Table III.

It is worth underlining that this proposed algorithm not only is easily adaptable to different operative conditions with a higher level of precision, but it is also able to analyze a video automatically, allowing to obtain the changes in the number of micro-particles in time for all the experiment duration.

In Fig. 7, the velocity trends $\langle V_y(t)\rangle$, obtained by the DPIV-based algorithm, in a time interval of 56 s for each type of micro-particles for the experimental condition $\{f_i = 0.1\,\text{Hz}, A = 0.1\,\text{ml/min}\}$ have been plotted. The oscillating trend of the velocity highlights the effects induced by the oscillating input flow. In particular, in Fig. 7, considering the same experimental condition, the amplitude of the velocity trend for the beads is lower than that found in the human and yeast cells due to the higher value of fluid density. Being heavier, they tend to lay down on the bottom of the micro-channel and offer greater resistance to the dragging force due to the density mismatch between the PBS fluid and the beads.[25]

Then, a comparison between the trends of the average velocity $\langle V_y(t)\rangle$ and the trend of the number of micro-particle $N_p(t)$ during some experiments, to detect the effects of a variable input force in the particle flow displacement, was performed. In Fig. 8, as an example the experimental condition $\{A = 0.15\,\text{ml/min}, f_i = 0.1\,\text{Hz}\}$ with the yeast cells is shown. In Fig. 8(a), the trend of the $\langle V_y(t)\rangle$ is compared with the trend of the $N_p(t)$. Three-time instants (t1, t2, t3) are considered and the relative frames and velocity fields were plotted, particularly it can be observed that

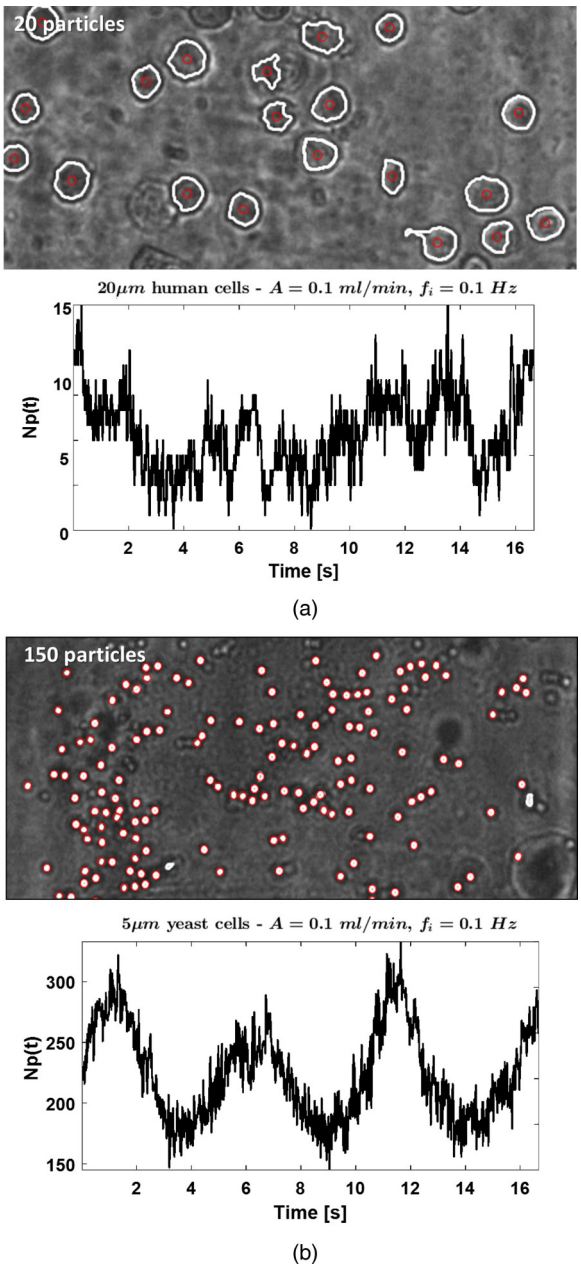

FIG. 6. The frames with the micro-particles detected marked in red circles and the mean number of micro-particles counted using the implemented algorithm per experiment: (a) human cells and (b) yeast cells in the experimental condition with $\{A = 0.1$ ml/min, $f_i = 0.1$ Hz$\}$.

- in t1, the number of particles is in a maximum $N_p(t1) = 300$ and the $\langle V_y(t)\rangle$ is near to 0 mm/s [see Fig. 8(b)];
- in t2, the number of particles is in a minimum $N_p(t2) = 150$ and the $\langle V_y(t)\rangle$ is negative [the particles are flowing from the bottom to the top, see Fig. 8(c) in blue arrow];
- in t3, the number of particles is in a minimum $N_p(t3) = 150$ and the $\langle V_y(t)\rangle$ is positive [the particles are flowing from the top to the bottom, see Fig. 8(d) in red arrow].

That is a consequence of the oscillatory hydro-dynamical stimuli imposed by the syringe pump flow rate: the particles tend to be highly concentrated when the stimulus reaches the zero value, conversely, they are dispersed during the rising phase of the stimulus (independently of the strength of the directionality).

To evaluate the hydrodynamic responses of the micro-particles, a comparison of the two parameters selected for the characterization of the processes, the range of the average velocity ($Range\langle V_y(t)\rangle$), and the amplitude in the peak spectrum at the stimulus frequency (A_{pk}) both un-normalized and normalized to the average number of particles ($\langle N_p(t)\rangle$) in the experiments was carried out in Secs. III C and III D.

B. Trend of micro-particle tracking and velocity

In order to overcome the hardware and software requirements for the development of a real-time approach through a CCD camera acquisition, the possibility of detecting the flows by using a photo-detector, which converts the acquired optical signal into an electrical signal, was investigated. In the implemented experimental setup, the photo-detector detects and measures the light variations acquired during the passage of the micro-particles inside the micro-channel. Then, it can convert them into voltage variations. The signals collected by the photo-detector were filtered by applying a notch filter at 50 Hz to remove the power supply component and down-sampled at 60 Hz in order to have the same sampling frequency as the camera. The photo-detector signals, after being filtered and down-sampled, have been compared with the velocity trends obtained by the DPIV-based algorithm as a proof of concept for further simplification and speed-up of the data acquisition and analysis. In Fig. 9, on the left column, the velocity trends and the photo-detector signals are superimposed for the yeast cells in the two experimental conditions with $\{A = 0.1$ ml/min, $f_i = 0.1; 0.2$ Hz$\}$. It is worth noticing a synchronous oscillating behavior with a phase shift due to the rounding of the down-sampling. That is confirmed by the spectral analysis on the right column shown in Fig. 9. The two frequencies of the external oscillating flow, imposed at the inlet, are undoubtedly detected and driving the changes of the cell flows.

C. Micro-particles classification by hydrodynamic response in time

The micro-particles hydrodynamic response in time domain was evaluated by computing the range of the velocity signal $\langle V_y(t)\rangle$ as shown in Eq. (3). Figure 10(a) shows the values of the velocity range ($Range\langle V_y(t)\rangle$) per experiment and Fig. 10(b) shows the values of the velocity range ($Range\langle V_y(t)\rangle$) per experiment normalized with respect to the average number of micro-particles ($\langle N_p(t)\rangle$) computed in the investigated area per experiment. Each point in the curve has been obtained as an average of the velocity values obtained under dynamical conditions maintained for 75 s. The stability of the signal ranges, shown in Fig. 7, confirms the robustness of the analysis in time and its reproducibility. In Fig. 10, the three curves are, respectively, for the micro-particles considered

TABLE III. The average number of micro-particles $\langle N_p(t)\rangle$ counted through the developed algorithm per experiment.

		Amplitude (ml/min)							
Micro-particles	Frequency (Hz)	0	0.03	0.04	0.05	0.07	0.1	0.15	0.2
Yeast cells	0.1	192	165	160	164	178	198	224	211
	0.2	…	…	…	216	233	227	…	231
Silica Beads	0.1	…	…	336	351	318	381	326	…
Human cells	0.1	…	…	15	20	12	45	14	…

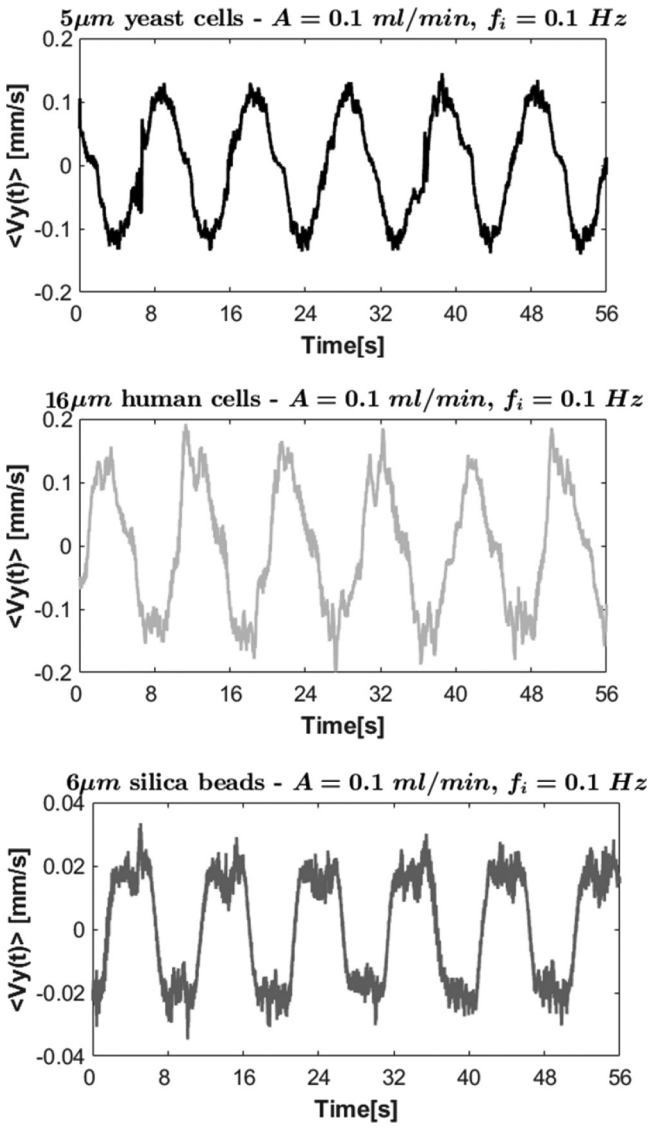

FIG. 7. For all the micro-particles, the velocity trends $\langle V_y(t)\rangle$ obtained in the experimental condition with $\{A = 0.1\,\text{ml/min}, f_i = 0.1\,\text{Hz}\}$.

(silica beads, yeast cells, and human cells) and each point per curve is correlated to a driving force by varying the amplitude of the external oscillating input flow strength A with a constant frequency $f_i = 0.1$ Hz.

In Fig. 10, it is evident a difference taking into account in both the plots two experimental conditions $\{A = 0.1\,\text{ml/min}, f_i = 0.1\,\text{Hz}\}$ and $\{A = 0.15\,\text{ml/min}, f_i = 0.1\,\text{Hz}\}$. In particular, in Fig. 10(a) for $A = 0.1$ the average of the velocity range in the case of human cells is greater than the one of the yeast cells, conversely in the second condition $A = 0.15$. In Fig. 10(b), after the normalization by the $\langle N_p(t)\rangle$, the values of the velocity range in the case of human cells are greater than the one of the yeast cells in both experiments. The value of the average velocity range for the silica beads is always the lowest. That can be correlated to the computational issues and the physical property of the particles .[48]

Assuming the density of the fluid and the particles close, after a transitory time, the particles' velocity follows the value of the fluid stream. In our experimental setup, the imposed input flow rate is oscillatory but the time needed to reach the maximum (to overcome the transitory phase) is greater than the oscillatory time. A difference of two orders between the stream velocity and the particles' velocity is obtained. Then, for example, in the case of $\{A = 0.1\,\text{ml/min}\}$ that corresponds, based on the micro-channel section, to a velocity stream of $v = 16$ mm/s, the maximum of the average of the velocity trend $\langle V_y(t)\rangle$ is for the human cell 0.2 mm/s, for the yeast cells 0.14 mm/s, and for the silica beads 0.03 mm/s. The value of $\langle V_y(t)\rangle$ obtained by computing the average in the space of $V_y(i, j, t)$ is affected by the number of moving particles in the area investigated: the greater the number of particles, the greater the value of the average velocity. In our experimental campaigns, three classes of particles in different concentrations were considered, and due to the oscillatory input strength, the number of particles in the area investigated is continuously changing. It is worth noticing, as reported in Table III, that the difference in the average number of particles is significant comparing the human cells vs the yeast cells and the silica beads. Even if the loss of the absolute value of the mean velocity range, the value of the velocity range after the normalization by the $\langle N_p(t)\rangle$ in the case of the human cells is greater than the one of yeast and silica beads that is coherent to the theoretical expectation. Indeed having the fluid and the particle at different densities, the buoyancy does not control ideally the particles' displacement in the stream and a difference in velocity can be detected. Based on the value of particles density reported in Table I and knowing the PBS density value

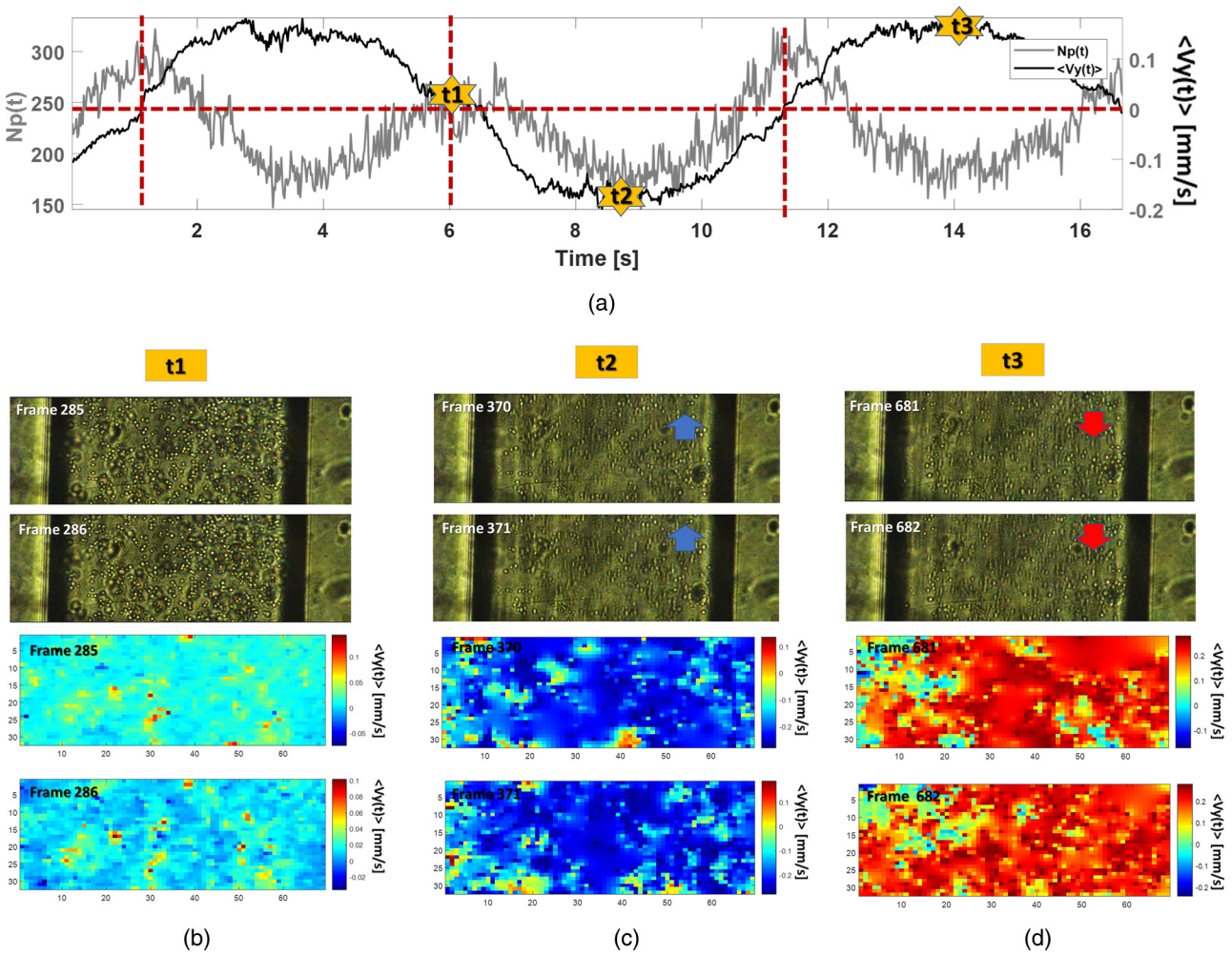

FIG. 8. DPIV-based analysis in the experimental condition with $\{A = 0.15\,\text{ml/min}, fi = 0.1\,\text{Hz}\}$ for the yeast cells. (a) The trend of the $\langle Vy(t)\rangle$ compared with the trend of the $Np(t)$. The frames and the relative velocity vector maps were reported in the conditions in which (b) the number of particles detected is maximum $[Np(t1) = 300]$ and the particles' velocity field is near 0 mm/s; (c) the number of particles minimum $[Np(t2) = 150]$ and the particles' velocity field negative (the particles are flowing from the bottom to the top) and (d) the number of particles minimum $[Np(t3) = 150]$ and the particles' velocity field positive (the particles are flowing from the top to the bottom).

equal to $1072\,\text{kg/m}^3$, the human cells would be faster than the yeast cells and the silica beads. Additionally, due to the friction, greater the diameter greater would be the particle velocity. In particular, it is noticeable that the normalized parameter $(Range\langle V_y(t)\rangle/\langle N_p(t)\rangle)$ increases as the amplitude of the flow increases. A parabolic interpolation of the points was performed per particles type, as shown for both the plots in Fig. 10. The parameter R^2, reported in the picture with the fitting equations, is always greater than 0.90 confirming the quality of the fitting. It is evident that the normalized parameter $(Range\langle V_y(t)\rangle/\langle N_p(t)\rangle)$ is sensitive to the dimensions of the micro-particles; indeed, the values of the human cells ($16\,\mu$m) are one order magnitude greater and increase faster than yeast cells ($5\,\mu$m) and silica beads ($6\,\mu$m). That leads to an immediate classification between the two classes of live cells. Additionally, it is worth to evidence a significant difference in the parabolic interpolation obtained for the yeast cells (live cells) and silica beads (synthetic particles), in spite of having the same dimension. That evidences the possibility of a differentiation correlated to other physical properties as the particles density and surface tissues.

To investigate the effect that can be induced in the process by changing the frequency f_i of the external oscillating input flow strength, the graph of Fig. 11(a), reports the normalized parameter $(Range\langle V_y(t)\rangle/\langle N_p(t)\rangle)$ for the experiments with yeast cells ($5\,\mu$m). In particular, the two curves are, respectively, for the driving force frequencies $f_i \in \{0.1; 0.2\}\,\text{Hz}$ and each point per curve is correlated to a driving force setting by varying the amplitude of the external oscillating input flow strength A. Also in this case, a good

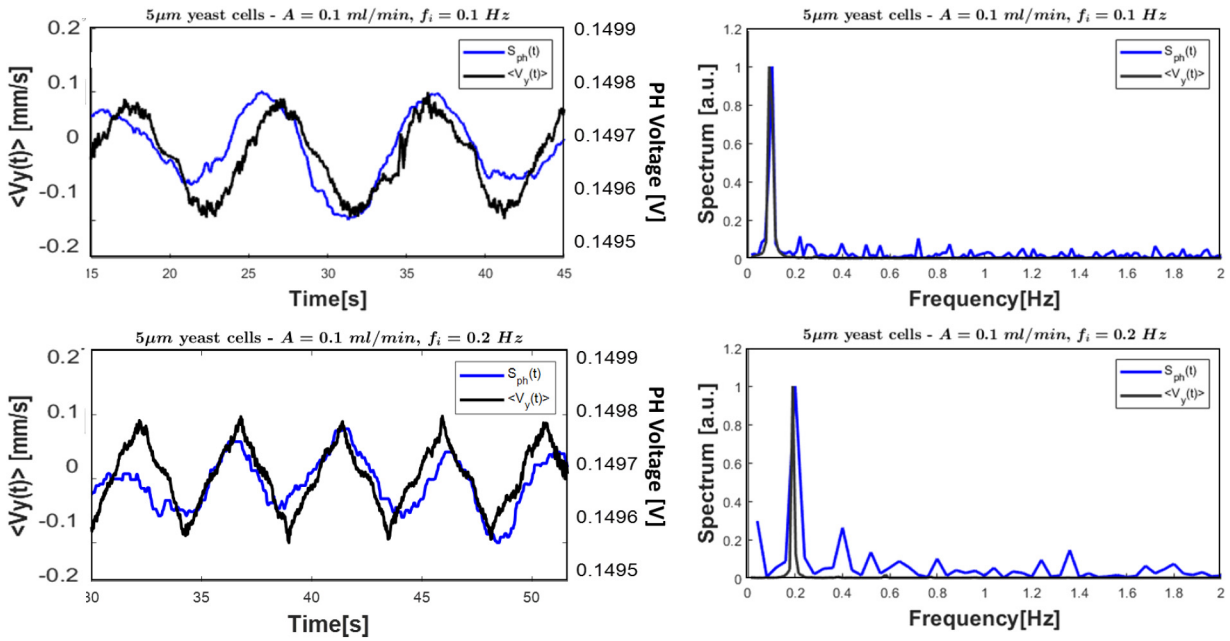

FIG. 9. The time course and the spectral analysis of the velocity trends extracted by the DPIV-based algorithm (in black) and the photo-detector signals (in blue) in the experimental conditions with $\{A = 0.1 - \text{ml/min}, f_i = \{0.1; 0.2\}\,\text{Hz}\}$ for the yeast cells.

interpolation with a parabolic function was obtained: the normalized parameter $(Range\langle V_y(t)\rangle/\langle N_p(t)\rangle)$ rises as the amplitude of the external oscillating input flow increases. The curves shift detected can be associated with the input frequency f_i: lower is the input frequency, greater is the signal range. This can be correlated to the inertial of the micro-particles flow, a slower input flow can be propagated more efficiently. Summarize, being the curves in Fig. 10(b), far apart for each other, it is worth to notice the possibility to detect, respectively, the difference in density of the three micro-particles and the effect determined by the driving force frequency.

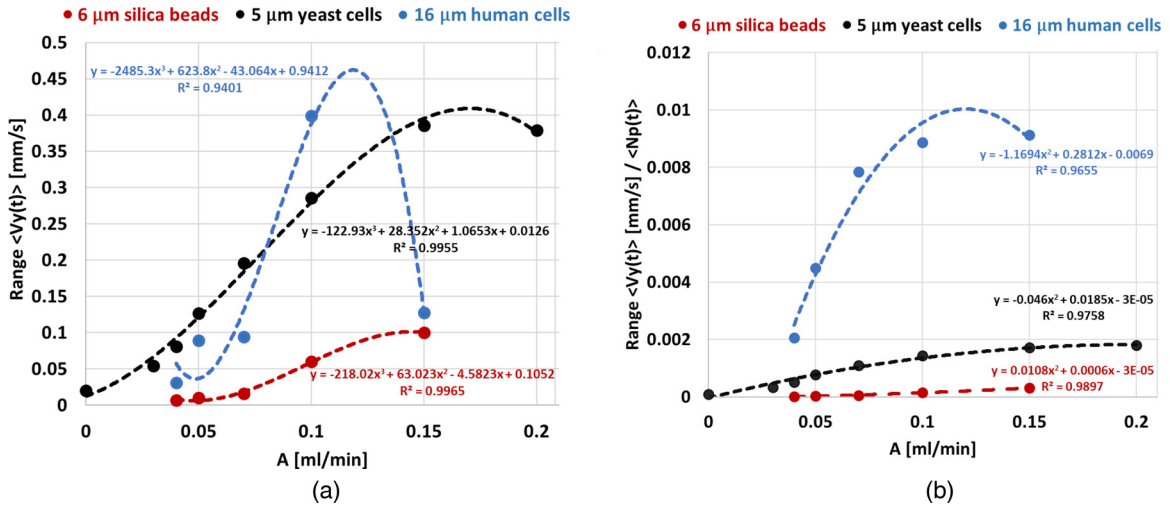

FIG. 10. (a) The parameter $(Range\langle V_y(t)\rangle)$ and (b) the normalized parameter $(Range\langle V_y(t)\rangle/\langle N_p(t)\rangle)$ varying the oscillating input flow strength at the inlet A for the three micro-particle types at $f_i = 0.1$ Hz.

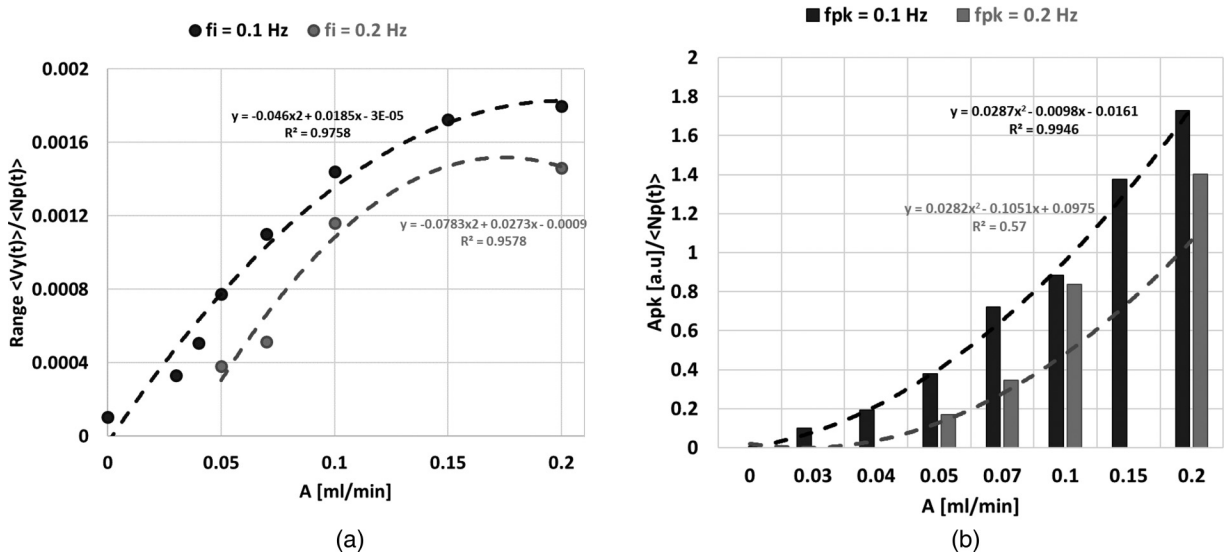

FIG. 11. The normalized parameters (a) ($Range\langle V_y(t)\rangle/\langle N_p(t)\rangle$) and (b) ($A_{pk}$) varying the oscillating input flow strength at the inlet A for the yeast cells at the input frequencies $f_{in} \in \{0.1; 0.2\}$ Hz.

D. Micro-particles classification by hydrodynamic response in frequency

The first experiment investigated in frequency domain was the $\langle V_y(t)\rangle$ for the single-phase PBS solution. It was fed at the inlet of the channel with an oscillating input flow with a frequency of $f_i = 0.1$ Hz and an amplitude of $A = 0.1$ ml/min. The frequency peaks identified were $f_{pk} \in \{6; 7.5\}$ Hz. They were correlated to the PBS background flow, assumed as process artifacts and neglected in the following data analysis.

The micro-particles hydrodynamic response in the frequency domain was evaluated by computing the spectrum of the velocity signal $\langle V_y(t)\rangle$ and of the velocity signal normalized for the average

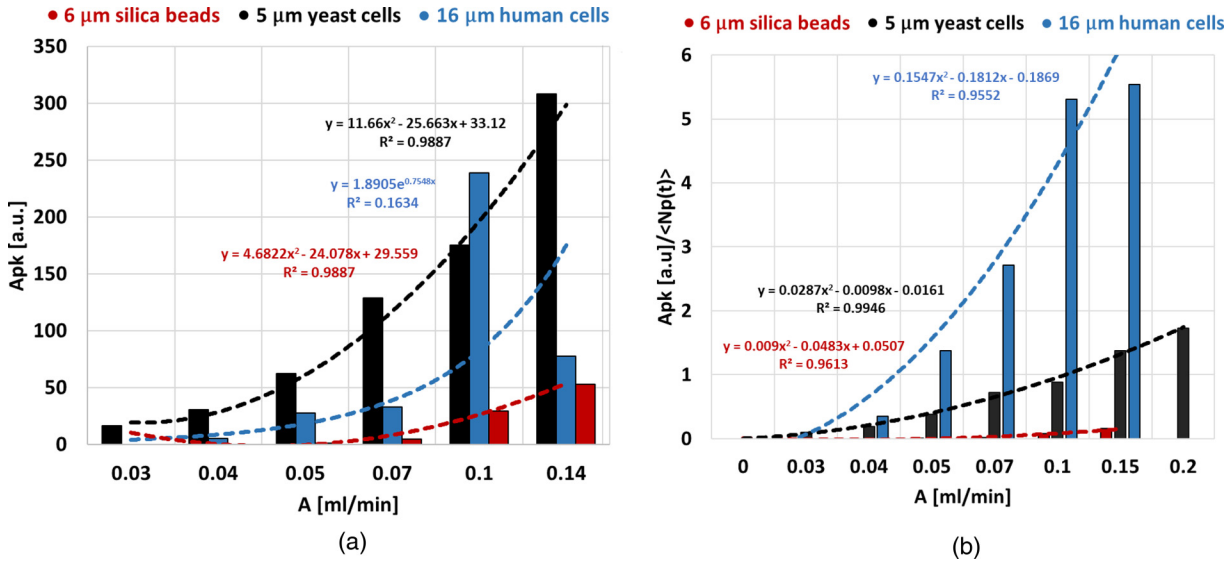

FIG. 12. Peak amplitude at $f_{pk} = 0.1$ Hz obtained by applying the spectrum to (a) the parameter ($\langle V_y(t)\rangle$) and (b) the normalized parameter ($\langle V_y(t)\rangle/\langle N_p(t)\rangle$) varying the oscillating input flow strength A at the inlet for the three micro-particles types at $f_i = 0.1$ Hz.

number of micro-particles. Figures 12(a) and 12(b) show the values of peak amplitude (A_{pk}) detected at $f_{pk} = 0.1$ Hz by applying the spectrum at the velocity signal $\langle V_y(t)\rangle$ and at normalized parameter ($\langle V_y(t)\rangle/\langle N_p(t)\rangle$) per cell type varying A. In the spectra at the low frequency range in Fig. 12, the dominant peak detected is at $f_{pk} = 0.1$ Hz, consistently with the frequency of the oscillating input flow considered $f_i = 0.1$ Hz. The amplitude of the peak at $f_{pk} = 0.1$ Hz increases with the rise of the flow strength A.

Considering all together the behaviors in the low frequency range, it is possible to conclude that for high external flow, the frequency induced by the pump is driving the hydrodynamic process, no other dynamics are relevant.

Extending this study to other experiments with the human cells and silica beads, similar behaviors were identified. In the experiments with the yeast cells where the oscillating input flow was set at $f_i = 0.2$ Hz, the dominant peaks in the low frequency were detected at $f_{pk} = 0.2$ Hz.

In Fig. 11(b), for the yeast cells, the amplitude of peaks $f_{pk} \in \{0.1; 0.2\}$ Hz normalized with respect to the average number of micro-particles ($\langle N_p(t)\rangle$) for the experiments with $f_i \in \{0.1; 0.2\}$ Hz is compared. In all the experiments, the normalized peak amplitude f_{pk} increases with external oscillating flow A and the values have been interpolated through parabolic functions. The amplitude of the normalized peaks for the experiments with human cells is bigger than those related to the other type of micro-particles; very small amplitudes with silica beads were observed. That enforces the results of the analysis in time domain and underlines the role played by the micro-particles physical properties in the hydrodynamic process.

IV. CONCLUSIONS

In this paper, the combination of two algorithms, a cell counting algorithm and a velocity algorithm, based on a Digital Particle Image Velocimetry (DPIV) method to investigate the collective behavior of micro-particles in response to hydrodynamic stimuli is presented.

The biological fluids were composed by three types of micro-particles, of different nature and sizes: the yeast cells (5 μm), the human cells (16 μm), and the silica beads (6 μm). They were injected in a micro-channel with different oscillating flows and the process was monitored in an investigated area by using an optical setup. The procedure proposed for the data analysis, designed to run automatically and adaptable to different experimental conditions, was based on the DPIV-based algorithm to compute the trend of the particle migration velocity in the investigated area and the custom counting algorithm to obtain the instantaneous micro-particles number. The velocity signals normalized with respect to the number of micro-particles were analyzed in both time and frequency domains showing the difference in the particles hydrodynamic responses to external stimuli and the possibility to associate them with the micro-particles physical properties. The frequency and the amplitude of the external oscillating driving force affect the micro-particles' flows and their setting can be modulated for stabilizing and investigating the micro-particles interaction.

Additionally, the signals collected by the photo-detector were compared with the velocity trends obtained by the DPIV-based algorithm as a proof of concept for a further simplification and speed-up of the data acquisition and analysis based on a simpler optical detection than the video recording. This could open the way to a greater simplification of the real-time process analysis.

The obtained results confirm fully the feasibility of the methodology to be integrated into a microfluidic Lab-on-Chip device for the investigation of the micro-particles interaction in pathological conditions. Rapid detection and characterization of different kinds of micro-particles would accelerate the diagnosis process and the development of targeted therapies. In future developments, thanks to the flexibility of the used platform, the algorithm will be optimized to be suitable for real-time detection in embedded systems.

ACKNOWLEDGMENTS

The research activity has been partially supported by University of Catania under the Grant Scheme PIACERI with the project MAF-moF "Materiali multifunzionali per dispositivi micro-optofluidici" and partially funded by European Union (NextGeneration EU), through the MUR-PNRR project SAMOTHRACE (No. ECS00000022).

AUTHOR DECLARATIONS

Conflict of Interest

The authors have no conflicts to disclose.

Author Contributions

Federica Torrisi: Data curation (equal); Formal analysis (equal); Investigation (equal); Methodology (equal); Software (equal); Validation (equal); Visualization (equal); Writing – original draft (equal); Writing – review & editing (equal). **Giovanna Stella:** Conceptualization (equal); Investigation (equal); Methodology (equal); Supervision (equal); Validation (equal); Visualization (equal); Writing – original draft (equal); Writing – review & editing (equal). **Francesca Guarino:** Conceptualization (equal); Investigation (equal); Methodology (equal); Resources (equal); Supervision (equal); Writing – original draft (equal); Writing – review & editing (equal). **Maide Bucolo:** Conceptualization (equal); Investigation (equal); Methodology (equal); Software (equal); Supervision (equal); Validation (equal); Visualization (equal); Writing – original draft (equal); Writing – review & editing (equal).

DATA AVAILABILITY

The data that support the findings of this study are available from the corresponding author upon reasonable request.

REFERENCES

[1]A. Cossarizza, H. D. Chang, A. Radbruch, M. Akdis, I. Andrä, F. Annunziato, P. Bacher, V. Barnaba, L. Battistini, W. M. Bauer, and S. Baumgart, "Guidelines for the use of flow cytometry and cell sorting in immunological studies," Eur. J. Immunol. **47**(10), 1584–1797 (2017).

[2]H. Cong, F. C. Loo, J. Chen, Y. Wang, S. K. Kong, and H. P. Ho, "Target trapping and *in situ* single-cell genetic marker detection with a focused optical beam," Biosens. Bioelectron. **133**, 236–242 (2019).

[3]P. K. Dagur and J. P. McCoy, Jr., "Collection, storage, and preparation of human blood cells," Curr. Protoc. Cytom. **73**(1), 5.1.1–5.1.16 (2015).
[4]S. Losserand, G. Coupier, and T. Podgorski, "Migration velocity of red blood cells in microchannels," Microvasc. Res. **124**, 30–36 (2019).
[5]A. Arboix, C. Jiménez, J. Massons, O. Parra, and C. Besses, "Hematological disorders: A commonly unrecognized cause of acute stroke," Exp. Rev. Hematol. **9**(9), 891–901 (2016).
[6]A. Vembadi, A. Menachery, and M. A. Qasaimeh, "Cell cytometry: Review and perspective on biotechnological advances," Front. Bioeng. Biotechnol. **7**, 147 (2019).
[7]S. Gupta, K. Ramesh, S. Ahmed, and V. Kakkar, "Lab-on-chip technology: A review on design trends and future scope in biomedical applications," Int. J. Bio-Sci. Bio-Technol. **8**(5), 311–322 (2016).
[8]A. M. Streets and Y. Huang, "Chip in a lab: Microfluidics for next generation life science research," Biomicrofluidics **7**(1), 011302 (2013).
[9]D. Mark, S. Haeberle, G. Roth, F. Von Stetten, and R. Zengerle, "Microfluidic labon-a-chip platforms: requirements, characteristics and applications," Chem. Soc. Rev. **39**, 1153–1182 (2010).
[10]M. Salve, K. Amreen, P. K. Pattnaik, and S. Goel, "Integrated microfluidic device with carbon-thread microelectrodes for electrochemical DNA elemental analysis," IEEE Trans. Nanobiosci. **21**, 322–329 (2021).
[11]H. Y. Tan and Y. C. Toh, "What can microfluidics do for human microbiome research?," Biomicrofluidics **14**(5), 051303 (2020).
[12]D. B. Weibel and G. M. Whitesides, "Applications of microfluidics in chemical biology," Curr. Opin. Chem. Biol. **10**(6), 584–591 (2006).
[13]D. Janasek, J. Franzke, and A. Manz, "Scaling and the design of miniaturized chemical-analysis systems," Nature **442**(7101), 374–380 (2006).
[14]G. Ochoa-Vazquez, B. Kharisov, A. Arizmendi-Morquecho, A. Cario, C. Aymonier, S. Marre, and I. López, "Microfluidics and surface-enhanced Raman spectroscopy: A perfect match for new analytical tools," IEEE Trans. Nanobiosci. **18**(4), 558–566 (2019).
[15]G. Aubry and H. Lu, "A perspective on optical developments in microfluidic platforms for *Caenorhabditis elegans* research," Biomicrofluidics **8**(1), 011301 (2014).
[16]L. Novak, P. Neuzil, J. Pipper, Y. Zhang, and S. Lee, "An integrated fluorescence detection system for lab-on-a-chip applications," Lab Chip **7**(1), 27–29 (2007).
[17]I. Grabowska, M. Sajnoga, M. Juchniewicz, M. Chudy, A. Dybko, and Z. Brzozka, "Microfluidic system with electrochemical and optical detection," Microelectron. Eng. **84**(5–8), 1741–1743 (2007).
[18]N. Azizipour, R. Avazpour, D. H. Rosenzweig, M. Sawan M, and A. Ajji, "Evolution of biochip technology: A review from lab-on-a-chip to organ-on-a-chip," Micromachines **11**(6), 599 (2020).
[19]K. D. Seo, B. K. Kwak, S. Sanchez, and D. S. Kim, "Microfluidic-assisted fabrication of flexible and location traceable organo-motor," IEEE Trans. Nanobiosci. **14**(3), 298–304 (2015).
[20]P. Chen, S. Li, Y. Guo, X. Zeng, and B. F. Liu, "A review on microfluidics manipulation of the extracellular chemical microenvironment and its emerging application to cell analysis," Anal. Chim. Acta **1125**, 94–113 (2020).
[21]J. Sibbitts, K. A. Sellens, S. Jia, S. A. Klasner, and C. T. Culbertson, "Cellular analysis using microfluidics," Anal. Chem. **90**(1), 65–85 (2017).
[22]M. Rothbauer, H. Zirath, and P. Ertl, "Recent advances in microfluidic technologies for cell-to-cell interaction studies," Lab Chip **18**(2), 249–270 (2018).
[23]A. G. Koutsiaris, D. S. Mathioulakis, and S. Tsangaris, "Microscope PIV for velocity-field measurement of particle suspensions flowing inside glass capillaries," Meas. Sci. Technol. **10**(11), 1037 (1999).
[24]C. D. Meinhart, S. T. Wereley, and J. G. Santiago, "PIV measurements of a microchannel flow," Exp. Fluids **27**(5), 414–419 (1999).
[25]A. G. Koutsiaris, "Digital micro PIV (μPIV) and velocity profiles *in vitro* and *in vivo*," in *The Particle Image Velocimetry—Characteristics, Limits and Possible Applications* (Intech Open, 2012).
[26]S. Pradeep and T. A. Zangle, "Quantitative phase velocimetry measures bulk intracellular transport of cell mass during the cell cycle," Sci. Rep. **12**(1), 1–14 (2022).
[27]T. N. Kim, P. W. Goodwill, Y. Chen, S. M. Conolly, C. B. Schaffer, D. Liepmann, and R. A. Wang, "Line-scanning particle image velocimetry: An optical approach for quantifying a wide range of blood flow speeds in live animals," PLoS One **7**(6), 1–13 (2012).
[28]M. Pereyra, A. Drusko, F. Krämer, F. Strobl, E. H. Stelzer, and F. Matthäus, "QuickPIV: Efficient 3D particle image velocimetry software applied to quantifying cellular migration during embryogenesis," BMC Bioinformatics **22**(1), 1–20 (2021).
[29]M. F. Sampedro, G. L. Miño, C. D. Galetto, and V. Sigot, "Spatio-temporal analysis of collective migration in vivo by particle image velocimetry," Phys. Biol. **18**(6), 066008 (2021).
[30]F. Cairone, D. Ortiz, P. J. Cabrales, M. Intaglietta M, and M. Bucolo, "Emergent behaviors in RBCs flows in micro-channels using digital particle image velocimetry," Microvasc. Res. **116**, 77–86 (2018).
[31]F. Cairone, D. Mirabella, P. J. Cabrales, M. Intaglietta, and M. Bucolo, "Quantitative analysis of spatial irregularities in RBCs flows," Chaos, Solitons Fractals **115**, 349–355 (2018).
[32]S. Sunardi, A. Yudhana, and S. Saifullah, "Identity analysis of egg based on digital and thermal imaging: Image processing and counting object concept," Int. J. Electr. Comput. Eng. **7**(1), 200 (2017).
[33]T. Liu, W. Wu, Chen,C. Sun, X. Zhu, and W. Guo, "Automated image-processing for counting seedlings in a wheat field," Precis. Agric. **17**(4), 392–406 (2016).
[34]N. Ab Azar, A. Babakhani, A. Broumandnia, and K. Sepanloo, "A novel method for detecting and counting overlapping tracks in SSNTD by image processing techniques," Radiat. Meas. **91**, 36–43 (2016).
[35]Y. H. Toh, T. M. Ng, and B. K. Liew, "Automated fish counting using image processing," in *International Conference on Computational Intelligence and Software Engineering* (IEEE, 2009), pp. 1–5.
[36]H. Zhang, C. H. Chon, X. Pan, and D. Li, "Methods for counting particles in microfluidic applications," Microfluid. Nanofluid. **7**(6), 739–749 (2009).
[37]D. Huh, W. Gu, Y. Kamotani, J. B. Grotberg, and S. Takayama, "Microfluidics for flow cytometric analysis of cells and particles," Physiol. Meas. **26**(3), R73 (2005).
[38]T. Hou, H. Chang, H. Jiang, P. Wang, N. Li, Y. Song, and D. Li, "Smartphone based microfluidic lab-on-chip device for real-time detection, counting and sizing of living algae," Measurement **187**, 110304 (2022).
[39]F. Schembri and M. Bucolo, "Periodic input flows tuning nonlinear twophase dynamics in a snake microchannel," Microfluid. Nanofluid. **11**, 189–197 (2011).
[40]F. Schembri, F. Sapuppo, and M. Bucolo, "Experimental identification of nonlinear dynamics in microfluidic bubbles flow," Nonlinear Dyn. **67**, 2807–2819 (2012).
[41]S. Gagliano, G. Stella, and M. Bucolo, "Real-time detection of slug velocity in microchannels," Micromachines **11**(3), 241 (2020).
[42]F. Cairone, S. Davi, G. Stella, F. Guarino, G. Recca, G. Cicala, and M. Bucolo, "3D-printed micro-optofluidic device for chemical fluids and cells detection," Biomed. Microdevices **22**, 37 (2020).
[43]A. G. Koutsiaris, "Loss of field of view due to optical mismatch at the inner diametric plane of cylindrical artificial microvessels," Results Opt. **8**, 100241 (2022).
[44]F. Cairone, S. Gagliano, and M. Bucolo, "Experimental study on the slug flow in a serpentine microchannel," Exp. Therm. Fluid Sci. **76**, 34–44 (2016).
[45]M. R. Green and J. Sambrook, "Estimation of cell number by hemocytometry counting," Cold Spring Harb. Protoc. **11**, 732–734 (2019).
[46]W. Thielicke and E. J. Stamhuis, "PIVlab towards user-friendly, affordable and accurate digital particle image velocimetry in MATLAB," J. Open Res. Software **2**(1), e30 (2014).
[47]C. A. Schneider, W. S. Rasband, and K. W. Eliceiri, "NIH Image to ImageJ: 25 years of image analysis," Nat. Methods **9**(7), 671–675 (2012).
[48]J. S. Turner and J. S. Turner, *Buoyancy Effects in Fluids* (Cambridge University Press, 1979).